

Three-Dimensional Particle Simulation Modeling of Ion Propulsion Plasma Environment for Deep Space One

J. Wang and D. Brinza

Jet Propulsion Laboratory, California Institute of Technology

Pasadena, CA 91109

M. Young

Department of Aerospace and Mechanical Engineering, University of Southern California

Los Angeles, CA 90089

Abstract

A fully three-dimensional particle-in-cell simulation model was developed to obtain ion propulsion charge-exchange plasma environment over the entire downstream-to-upstream region for the Deep Space 1 (DS1) spacecraft. Simulations are compared with in-flight measurements of charge-exchange plasma from the Ion Propulsion Diagnostics Subsystem on DS1, and the results show an excellent agreement. It is found that the plasma environment of DS1 spacecraft is dominated by the charge-exchange plasma from the plume. For a typical ion thruster operating condition, the charge exchange plasma near the spacecraft surface has a density ranging from 10^6 cm^{-3} at the thruster end to 10^4 cm^{-3} at the opposite end, and a current density ranging from $10^{-7} \text{ A/cm}^{-2}$ to $10^{-9} \text{ A/cm}^{-2}$. It is shown that for an interplanetary spacecraft with a moderate charging potential, charge-exchange ion backflow is through an expansion process similar to that of the expansion of a mesothermal plasma into a vacuum.

1 Introduction

Ion propulsion devices are valued as a high-specific impulse class of space propulsion. NASA's New Millennium Deep Space One (DS1) marks the beginning of interplanetary missions using spacecraft operated with ion propulsion. Using a 30cm diameter Xenon ion thruster as its primary propulsion, DS1 successfully flew by asteroid Braille on July 28, 1999, and is currently on a trajectory for a possible encounter with comet Borrelly in 2001.

An ion thrusters propels a spacecraft by continuously emitting a partially ionized gas. An ion thruster plume is composed of propellant efflux (high energy beam ions, neutralizing electrons, and un-ionized neutrals that escaped through the ion optics and from the neutralizer), nonpropellant efflux (material sputtered from thruster components and the neutralizer), and a low-energy charge-exchange plasma generated by collisions between the beam ions and the neutrals within the plume. It is well known that both the low energy charge-exchange ions and the ionized sputtered particles can be pushed out of the plume by local electric field and backflow to interact with spacecraft [Carruth, 1981, 1982].

As the propellant charge-exchange ion is the dominant backflow species, the characteristics of ion thruster plume-spacecraft interactions are primarily determined by the charge-exchange plasma environment. Charge exchange ions can affect spacecraft charging by interacting with the solar arrays and any exposed conducting surface. Charge exchange ions can affect space plasma measurements performed on-board by interacting with the ambient plasma and by dominating the local plasma environment surrounding spacecraft. For a Xenon ion thruster, the Xenon charge-exchange ions do not directly contaminate spacecraft surface because Xe is not a contaminating species. Spacecraft contamination is caused by the backflow of sputtered grid material, which is molybdenum. Deposition of molybdenum particles can cause property changes on thermal and optical surfaces. However, the charge exchange plasma may play an important role in the backflow of contaminating species through its effects on the electric field and plasma sheath surrounding spacecraft, which in turn controls the trajectories of any ionized particles near spacecraft. Effects from charge exchange plasma interactions are especially important for an interplanetary spacecraft. This is because the density of the solar wind plasma is only about 1 to 10 particles per cm^3 , and thus the spacecraft plasma environment will be dominated by the charge-exchange plasma from the thruster plume.

The DS1 mission provides the first ever comprehensive in-flight investigations of ion thruster plume-spacecraft interactions. DS1 carries an integrated set of ion propulsion diagnostic package, Ion propulsion Diagnostic System (IDS), and a state-of-the-art plasma sensor, Plasma Experiment

for Planetary Exploration (PEPE). Both IDS and PEPE have produced high quality data concerning ion thruster plume-spacecraft interactions. DS1 measurements of ion propulsion plasma environment were recently reported by *Wang et al.*[2000]. DS1 measurements of ion propulsion contamination are reported by *Brinza et al.*[2000] in the same issue. Subsequent publications of further data analysis work are also being planned. Since IDS and PEPE make only single point measurements, modeling is essential to provide a more complete description of plume-spacecraft interactions. A set of computer particle simulation based numerical models has been developed to assist the data analysis and interpretation. This paper reports results from a modeling investigation of ion propulsion plasma environment of DS1.

Computer particle simulation has proven to be the best tool available for modeling plasma plume-spacecraft interactions. Recently, several computer particle simulation models have been developed for ion thruster plume [*Samanata Roy*,1996; *Wang et al.*,1996; *Katz et al.*,1997; *VanGilder et al.*,1997]. However, most of the simulation studies published so far have focused on the region downstream of the thruster exit. None of the published studies have modeled the charge-exchange plasma in the entire upstream region of the thruster exit. It is the upstream region that is most relevant for assessment of effects from plume-spacecraft interactions.

In this paper, we present a 3-dimensional particle-in-cell model which simulates charge-exchange ion interactions over an entire downstream-to-upstream region surrounding a spacecraft. Using measured in-flight ion thruster operation parameters as input, this model is applied to obtain ion propulsion induced plasma environment surrounding DS1. Section 2 briefly describes the DS1 spacecraft, ion thruster operation parameters, and in-flight measurements of the ion propulsion charge-exchange plasma. Section 3 discusses the simulation model. Section 4 presents simulation results and compares them with in-flight measurements. Section 5 contains conclusions.

2 DS1 Spacecraft and In-Flight Measurement

2.1 Spacecraft

Figure 1 illustrates the DS1 spacecraft with deployed solar arrays. The DS1 spacecraft bus plus the propulsion module is essentially a hexagon cylinder with about 1.6m in height and 1.2m in diameter. In the local coordinate shown in Figure 1, the spacecraft orientation is such that the thrust vector is along the $-z$ axis and the solar array face is almost always facing the $+x$ axis.

The SCARLET (Solar Concentrator Arrays with Refractive Linear Element Technology) solar array has a voltage span of 100 volts. The solar array support panel is made of graphite/epoxy

facesheets on aluminum honeycomb. The concentrator connectors are covered by insulating materials to prevent arcing. Both the spacecraft and the solar array support panel are grounded at the 0 volt end of the SCARLET solar array.

A close-up view of the DS1 spacecraft with the PEPE and IDS instrument is illustrated in Figure 1 of Brinza et al.[2000] in this issue. The plasma sensors of IDS include a retarding potential analyzer (IDS-RPA) and a planar Langmuir probe (IDS-LP1). IDS-RPA and IDS-LP1 are co-located at about 75 cm from the thruster centerline. PEPE is located on the surface at the opposite end from the thruster. For detailed discussions of the IDS and PEPE instruments, the readers are referred to [Wang et al.,2000] and [Brinza et al.,2000].

2.2 Ion Thruster Plume

The 30 cm diameter NSTAR (NASA Solar electric propulsion Technology Application Readiness) xenon ion thruster used on DS1 has an input power range of 500 to 2300 W. The propellant Xe^+ ions are accelerated through a molybdenum grid to form a beam with an energy E_b up to 1100 eV (exit beam velocity of $v_b \simeq 3.5 \times 10^6$ cm/s), and a current I_b up to 1.8 A. At full thrust level, the thruster produces a thrust of 92 mN and a specific impulse of about 3100s. Measurements have shown that the propellant ions form a divergent beam with a divergence half angle of about 15° to 20° due to the curvature of the thruster exit surface. The ion beam is kept quasi-neutral by electrons emitted from the neutralizer.

The propellant that remains un-ionized flows out of the thruster exit in free molecular flow with a thermal speed corresponding to the thruster wall temperature of $T_w \sim 500$ K (0.04 eV). The density of the neutral plume typically remains quasi-steady due to the low charge-exchange collision rate. One can estimate the average neutral density at thruster exit, n_{n0} , from the measured main flow rate, cathode flow rate, and the discharge propellant efficiency η_d . Assuming that the un-ionized propellant exits through the grids in free-molecular flow with a temperature close to that of the thruster discharge chamber walls T_w , n_{n0} can be calculated from:

$$n_{n0} = \frac{\dot{N}_n}{A_n \sqrt{8kT_w / \pi m_{Xe}}} \quad (1)$$

where \dot{N}_n is the number of Xe particles per second, and is converted from the discharge chamber flow rate, $\dot{m}_d = (1 - \eta_d)(\dot{m}_m + \dot{m}_c)$. A_n is the flow-through area through the grids and is about 0.24 of the thruster exit area for the NSTAR thruster.

Charge-exchange collisions will occur between the beam ions and the neutrals. The average

charge exchange ion production rate at the thruster exit is given by

$$\frac{dn_{cex0}}{dt} = n_{b0}n_{n0}v_b\sigma_{cex} \quad (2)$$

where n_{b0} is the average beam ion density at the thruster exit, $n_{b0} = I_b/(ev_bA)$, and σ_{cex} the charge-exchange ion collision cross section. σ_{cex} can be estimated from curve fitting of the measured collision cross section for $Xe^+ - Xe$ charge-exchange [Rapp,1962; Samanta Roy et al.,1996]:

$$\sigma_{cex} = (k_1 \ln v_b + k_2)^2 \times 10^{-16} \text{ cm}^2 \quad (3)$$

where v_b is beam ion velocity with unit in m/s, $k_1 = -0.8821$, and $k_2 = 15.1262$.

2.3 Engine Parameter and In-Flight Measurement

The NSTAR ion thruster can be operated over a wide range of engine parameters [Polk et al.,1999]. A thruster flight throttle table is also listed in Table 1 of [Brinza et al.,2000]. For comparison with in-flight measurement, we consider a typical engine operating condition in this paper, mission throttle level (ML) 83. ML 83 is chosen because it is one of the highest power levels at which the thruster has operated during the entire DS1 mission. It is also an operating condition which was monitored by simultaneous IDS and PEPE measurements [Wang et al.,2000]. ML 83 has an engine input power of 1.82 kW and a specific impulses of 3189s. From flight data, we find the values of beam current I_b , beam ion energy E_b , and discharge propellant efficiency η_d for ML 83 to be $I_b \simeq 1.40\text{A}$, $E_b \simeq 1095\text{eV}$, and $\eta_d \simeq 0.88$, respectively [Wang et al.,2000]. Using these data, one readily calculates the beam plasma density, neutral density, and the charge-exchange ion production rate near the thruster exit. The results are listed in Table 1.

The induced plasma environment for ion thruster operation at ML 83 was measured by both IDS and PEPE on January 22, 1999 [Wang et al.,2000]. From IDS measurements, we have obtained the average plume potential Φ_p with respect to the potential of the spacecraft ground Φ_{scg} , and the local plasma conditions at the location of IDS, including the plasma potential Φ_{IDS} with respect to Φ_{scg} , the charge-exchange ion current density J_{cex} and number density n_{cex} , average energy of charge exchange ions E_{cex} , and electron temperature T_e . The results are listed in the upper part of Table 2. PEPE also observed the Xenon charge-exchange ions, and has conclusively shown that charge-exchange ions from the plume can backflow to the opposite side of spacecraft. PEPE data is still being analyzed to obtain physical parameters for the charge-exchange plasma.

PEPE has a lower energy cut-off of ± 8 Volt for instrument protection. The DS1 spacecraft floating potential cannot be determined from PEPE measurements of the solar wind because

it falls under this lower energy cut-off threshold. PEPE measurements during the mission has suggested that any change in spacecraft potential due to ion thruster operation is within the ± 8 Volt range.

3 3-Dimensional Particle Simulation Model

A 3-dimensional electrostatic particle-in-cell (PIC) code is developed to solve self-consistently the particle trajectories and space charge for the charge-exchange plasma, and the electric field surrounding the spacecraft. Since our emphasis here is on charge exchange ion backflow, only the charge-exchange ions are treated as test particles.

The basic formulation for charge-exchange ion production is similar to that used in [Samanta Roy et al.,1996]. The density distribution of the propellant beam ions $n_b(\vec{x})$ is modeled by an analytically profile because the propellant beam ions follow a ballistic trajectory due to their high energy. We assume that the radial current density profile of the beam ions to follow a parabolic core and an exponential wing. The density distribution of the neutral plume $n_n(\vec{x})$ is also modeled analytically as that of a free molecular flow from a point source located at one thruster radius r_T behind the thruster exit. The density distribution of the neutral plume is given by:

$$n_n(R, \theta) = an_{n0}(1 - (1 + (\frac{r_T}{R})^2)^{-1/2}) \cos \theta \quad (4)$$

where R is the distance to the point source, θ is the angle between R and the downstream axis, and a is a correction factor. Using the analytical profiles for the beam ions and the neutral plume, one obtains the spatial distribution of the charge-exchange ion production rates

$$\frac{dn_{cex}}{dt} = n_b(\vec{x})n_n(\vec{x})v_b\sigma_{cex} = \frac{n_b(\vec{x})}{n_{b0}} \frac{n_n(\vec{x})}{n_{n0}} \left(\frac{dn_{cex0}}{dt} \right) \quad (5)$$

where dn_{cex0}/dt is the average charge exchange ion production rate at the thruster exit. The values n_{b0} , n_{n0} , and dn_{cex0}/dt can be obtained from ion engine operation parameters, as discussed in Section 2.2.

Test particles representing charge-exchange ions are generated at each time step according to the volumetric production rate of eq(5). The trajectory of each charged particle is integrated from

$$m \frac{d\vec{v}}{dt} = \vec{F} = q(\vec{E} + \vec{v} \times \frac{\vec{B}}{c}), \quad \frac{d\vec{x}}{dt} = \vec{v} \quad (6)$$

using a standard leapfrog scheme. A “gather” step interpolates the fields from grid points to particle positions, and a “scatter” step deposits the charge of each test particle to grid points.

A commonly used assumption in plasma plume modeling is that the electron density may be described by the Boltzmann relationship [Samanta Roy et al.,1996; VanGilder et al.,1999]. In principal, one may employ full particle simulations using test particles to represent both the ions and electrons. Such an approach has been applied recently for field-emitter electric propulsion thruster plume [Tajmar and Wang,2000]. Full particle simulations typically require the use of an artificial ion to electron mass ratio to reduce the difference between the electron and ion time scales for computational reasons. The plasma plume is a mesothermal plasma i.e., the directed ion velocity is much larger than the ion thermal velocity but much smaller than the electron thermal velocity. To correctly model a mesothermal plasma in a full particle simulation model, an extremely large ion to electron mass would need to be used. This makes it computationally very ineffective and expensive to model charge-exchange plasma interactions using full particle simulations. Hence, the assumption of a Boltzmann electron distribution is also adopted in this study.

We take the reference point for the Boltzmann relation to be the thruster exit condition, and the electron density distribution is given by

$$n_e = n_{e0} \exp\left(\frac{\Phi - \Phi_{p0}}{T_e}\right) \quad (7)$$

where $n_{e0} = n_{b0}$ is the average plasma density at thruster exit and Φ_{p0} is the plume potential near thruster exit. In previous studies such as [Samanta Roy et al.,1996a], the reference point is taken to be the ambient plasma condition, implying that the neutralization of charge exchange ions is provided by the ambient electrons. Such an assumption is not appropriate here because the DS1 ion thruster operates in the interplanetary plasma environment where the median observed solar wind density is $n_{sw} \simeq 6.9 \text{ cm}^{-3}$ [Gosling,1999]. At such a low density, the ambient plays no role in neutralizing the charge-exchange ions. The nature of this model is such that both the electron temperature T_e and the plume potential Φ_{p0} need to be specified by other means. In our simulations, the values for T_e and the plume potential with respect to spacecraft, $\Phi_{p0} - \Phi_{sc}$, are taken from in-flight IDS measurements, as discussed in section 2.3.

The self-consistent electric field and space charge are obtained from the Poisson's equation

$$\nabla^2 \Phi = -4\pi e(n_i - n_{e0} \exp\left(\frac{\Phi - \Phi_{p0}}{T_e}\right)) \quad (8)$$

where n_i is the total ion charge density. To solve this nonlinear Poisson's equation in a 3-dimensional space, we have employed a dynamic alternating direction implicit (DADI) method [Doss et al.,1979; Hewett et al.,1992] with a defect correction using the Douglass-Gunn operator splitting [Douglas and Gunn,1964]. This DADI method was chosen over other algorithms for

its increased stability properties over fully explicit methods and its relatively simple tridiagonal system of equations produced by the partially implicit nature of the method. The alternating direction implicit (ADI) method first introduces a fictitious time derivative. An initial guess, typically the potential at the previous real time level, is then advanced until steady-state conditions are reached. At the steady state condition the time derivative vanishes leaving the original equation. The ADI method splits the spatial operator along the coordinate directions. Each time step is therefor split into a sequence of sub-steps, each with only one operator acting implicitly. The defect correction implementation of the Douglass-Gunn operator splitting [Douglas and Gunn, 1964] is given by

$$\left(-\frac{1}{dt} + \frac{H}{2}\right)d' = \text{Res}(S^n), \left(-\frac{1}{dt} + \frac{V}{2}\right)d'' = -\frac{1}{dt}d', \left(-\frac{1}{dt} + \frac{N}{2}\right)d^* = -\frac{1}{dt}d'' \quad (9)$$

where H , V , and N are the spatial operators for each coordinate direction, Res is the residual operator, and d is the defect. The spatial operators are generated through second order central differencing. The solution at the new time-step is given by

$$S^{n+1} = S^n + d^* \quad (10)$$

The nonlinear source term is updated after each application of the HVN set of operators. Dynamic ADI automatically adjusts the fictitious time-step by comparing two separate solutions to the problem. The first solution, \bar{S}^{n+1} , is obtained from a single application of the HVN set of operators. The second, typically more accurate, solution, S^{n+1} , is obtained from completing two sequential applications of the HVN set of operators, each with half the fictitious time-step. A test parameter is then used to estimate the amount of error associated with taking the larger time-step to calculate the acceleration factor for the next fictitious time-step:

$$TP = \frac{||S^{n+1} - \bar{S}^{n+1}||}{||S^{n+1} - S^n||} \quad (11)$$

Each spatial grid-point, including the boundaries, can be defined as open or solid point allowing for physical objects inside the computational domain and grid-point specific Neumann or Dirichlet conditions on the boundary.

The simulation setup is shown in Figure 2. We model the DS1 spacecraft as a hexagon cylinder and the solar array as a thin plate. The hexagon cylinder and the backside of the solar array are conductors with a uniform spacecraft potential Φ_{sc} . The front face of the solar array is covered by glass, and thus an insulator. It typically has a surface voltage of about $-T_e$, where T_e is the electron temperature of the ambient electrons in the unit of eV. This solar array model is sufficient for our purpose because all the high-voltage connectors on the solar array have been covered by

insulating materials. Moreover, any potential leakage from the edge of the solar array will be shielded out within a distance of a few Debye length by the charge-exchange plasma.

By taking into account of geometric symmetry, the simulation presented in this paper includes only a quarter-size of the spacecraft and part of one solar array. We take the simulation domain to be in the $-x$, y , and $-z$ region. The origin of the coordinate system is at $(-x, y, -z) = (1, 1, 1)$. The spacecraft centerline is placed at the $(-x, y) = (1, 1)$ axis and thrust vector is along the $-z$ direction. The solar array panel lies on the $-x = 1$ boundary. Its surface facing into the simulation domain is the backside of the solar array. The conditions at $-x = 1$ and $y = 1$ boundaries are that for a symmetric face. All other boundaries are considered open boundaries. Since computationally it is not feasible to set the simulation domain large enough for the outer boundary to be the undisturbed ambient, a Neumann condition $\nabla\Phi_n = 0$ is used at all open boundaries.

Out of considerations for computational efficiency and speed for large scale 3-dimensional simulations, the computational grid is chosen to be a uniform grids. To capture the details in the high density region near thruster exit, one could use an adaptive grid such as tetrahedral cells or non-orthogonal grids. However, these PIC codes are computationally significantly more expansive than a standard orthogonal grid PIC code because of the added complexity and memory references needed for particle tracking [Wang *et al.*, 1999]. Our main interest is in the upstream region where the particle density is significantly lower than that at thruster exit. Hence, we find that it is much more efficient to apply the computational resources on tracking more particles to increase the particle statistics in the backflow region.

4 Results and Discussions

In this section, we present simulation results for the ion engine operating condition ML 83. As discussed in last section, the input parameters for the simulation model are n_{b0} , n_{n0} , dn_{cex0}/dt , T_e , and $\Phi_{p0} - \Phi_{sc}$. The values for n_{b0} , n_{n0} , and dn_{cex0}/dt are obtained from ion engine operation parameters, and are listed in Table 1. IDS measures T_e and the average plume potential near thruster exit Φ_p with respect to the spacecraft ground Φ_{scg} . To a good approximation, we assume $\Phi_{p0} - \Phi_{sc} \simeq \Phi_p - \Phi_{scg}$. The measured values for T_e and $\Phi_p - \Phi_{scg}$ are listed in Table 2.

In the simulation, the potential on the spacecraft and solar array surface is set at Φ_{sc} . We emphasize that the electric potential of the spacecraft-plume system is floating with respect to the ambient. Hence, only the relative potential difference $\Phi_{p0} - \Phi_{sc}$ is a meaningful parameter. The relative potential difference between Φ_{sc} and the ambient potential is not known *a priori*.

However, when a steady state is reached, the potential at simulation outer boundary represents the ambient potential with respect to the spacecraft.

In the simulations, the grid resolution is chosen mainly to resolve the charge exchange plasma in the backflow region. Here, the grid resolution is taken to be $d_{cell} \simeq 6\text{cm}$ and the the number of grid points used are $43 \times 43 \times 71$. At steady state, the number of test particles in the simulation domain is 5 million. The large number of test particles is needed in order to obtain meaningful statistics in the backflow region. The entire simulation can be completed in about 5 CPU hours on a Cray SV1-1A supercomputer. Simulations were also performed for different grid resolutions and number of test particles to ensure that the simulation results are not affected by simulation parameters.

In the following discussions, the notations x , y , and z are understood to be variables normalized by the cell size d_{cell} . The spacecraft bus is a hexagon cylinder along the z direction, located at $23 \leq -z \leq 48$. The solar array is a flat plate bounded by $18 \leq -z \leq 44$ and $22 \leq y \leq 44$ on the $-x = 1$ face. The thruster exit center is at $(-x, y, -z) = (1, 1, 49)$.

Figure 3 shows the locations of the spacecraft and the solar array on the $x = -1$ plane along with beam ion density contours calculated from the beam ion model, neutral plume density contours for the from the neutral plume model, and the contours for the charge-exchange ion production rate calculated from eq(5).

In Figures 4 and 5, we show simulation results on a zy plane cutting through the spacecraft and thruster center at $-x = 1$ and on a zy plane near spacecraft outer boundary at $-x = 10$, respectively. In Figures 6 and 7, we show simulation results on a zx plane cutting through the spacecraft and thruster center at $y = 1$ and on a zx plane at $y = 30$, respectively. All these figures show potential contours, ion density contours, the directions of electric fields $\vec{E}/|E|$, and the directions of charge-exchange ion current density $\vec{J}_{cex}/|J_{cex}|$.

Since the ion beam is quasineutral and the beam ion energy E_b is much larger than the potential from spacecraft, the beam ions are not influenced by the potential field. In contrast to the beam ions, the low energy charge exchange ions are greatly influenced by the electric field in the plume. Since the electrons are much more mobile than ions, the beam center has a higher potential (Figure 4a,b and Figure 6a,b). As a result, charge exchange ions produced in the beam flow radially outward the beam region as shown in (Figure 4c,d and Figure 6c,d). The space charge carried by the outflowing charge-exchange ions generates a wing structure near the thruster exit in both the potential contours and ion density contours (The a and c panels in Figures 4 through 7).

Once outside the beam region, the charge exchange ions start to expand and interact with the spacecraft. As evident from the c and d panels in Figure 4 through 7, an expansion fan structure is generated at the edge of thruster exit surface at $-z = 48$. The velocities of the charge exchange ions are turned gradually from the radially outward direction in the downstream region to the $+z$ direction near spacecraft surface.

We find that the problem of charge-exchange plasma backflow has the same physics underlying the problem of plasma expansion into a vacuum or plasma wake (see, for example, [Wang and Hastings, 1991a,b; and references there in]). Unless the spacecraft is highly charged, the fundamental process is governed by the expansion of a mesothermal plasma. The plasma expansion is similar to the Prandtl-Meyer expansion of a supersonic gas flow over a convex corner [Wang and Hastings, 1991a]. The expansion fan is a presheath for the spacecraft, which turns the trajectories of the charge-exchange ions into the upstream direction. until they enter into the sheath of spacecraft.

As a result of charge-exchange ion backflow, the spacecraft sees a substantial charge exchange ion density. In Figure 8, we plot the potential, charge exchange ion number density, and current density along several x axis in the $y = 1$ plane. The charge-exchange ion density near spacecraft ranges from 10^6 cm^{-3} at $-z = 50$ (the thruster end) to 10^4 cm^{-3} at $-z = 24$ (the opposite end). As the charge-exchange plasma density near spacecraft is at least about three orders of magnitude larger than the solar wind plasma density, the plasma environment of DS1 spacecraft is completely dominated by the charge-exchange plasma in the plume.

The thickness of plasma sheath surrounding a spacecraft is about a few Debye length of the surrounding plasma. The Debye length under typical solar wind conditions is on the order of 10 m. The Debye length in a charge-exchange plasma environment with a density of 10^4 cm^{-3} is on the order of 10 cm. Hence, ion thruster operation will reduce the thickness of the plasma sheath surrounding DS1 from $O(10)$ m to $O(10)$ cm. As a result, the spacecraft potential will be shield in the immediate vicinity. The thin sheath is evident in both the potential contour plots and in Figure 8a.

The simulation also suggests the spacecraft floating potential relative to the ambient. In Figure 8a, the spacecraft potential is set at $\Phi_{sc} = 0$ V. The potential at the simulation boundary is floating with respect to the spacecraft. Figure 8a suggests that the spacecraft potential is about -5 V with respect to the plasma at “infinity”.

In Table 2, we compare simulation results with IDS measurements. The simulation results are taken at a grid point at a location similar to that of IDS. We find that the charge-exchange

plasma density matches each other within a factor of 1.2, and the current density matches each other within a factor of 1.7. The major uncertainties in the simulation model include the following: the assumption that the input value of $\Phi_{p0} - \Phi_{sc}$ is taken to be the measured value of $\Phi_p - \Phi_{scg}$; the negligence of any differential charging that may present; and the validity of Boltzmann relationship for the electrons. Considering all the simplifications and assumptions involved in our simulation model, the agreement between the simulation and measurement is very remarkable.

5 Conclusions

A fully 3-dimensional particle-in-cell simulation model of ion propulsion plasma plume was developed. This model was applied to obtain the induced charge-exchange plasma environment over the entire downstream-to-upstream region surrounding the DS1 spacecraft. Using the in-flight ion thruster operating condition as input parameters, the simulation results and measured charge-exchange ion parameters from IDS are in excellent agreement.

For an interplanetary spacecraft, the physics underlying charge-exchange plasma spacecraft interaction is the same as that of plasma expansion into a vacuum or plasma wake. Once outside the beam, the charge-exchange ions undergo an expansion process which gradually turns their velocity vector from the radially outward direction to the upstream direction. As a result, the DS1 spacecraft is immersed in a dense charge-exchange plasma environment. Near the spacecraft surface from the thruster end to the opposite end, the charge exchange plasma density ranges from 10^6 cm^{-3} to 10^4 cm^{-3} , and the charge-exchange current density ranges from $10^{-7} \text{ A/cm}^{-2}$ to $10^{-9} \text{ A/cm}^{-2}$, for a typical ion thruster operating condition. As the charge-exchange plasma density near spacecraft is at least about three orders of magnitude larger than the solar wind plasma density, the plasma environment of DS1 spacecraft is completely dominated by the charge-exchange plasma in the plume. Since the spacecraft potential is shielded by the thin sheath in the charge-exchange plasma, spacecraft charging potential will not have any significant effect on the backflow of the ionized molybdenum particles sputtered from the thruster.

Acknowledgments

We acknowledge many helpful discussions with R. Samanta Roy of IDA, I. Katz of Maxwell Labs, D. Young of U. Mich., S.P. Gary and J. Nordholt of LANL, B. Goldstein, P.C. Liewer, and J. Polk of JPL, and D. Hewett of LLNL. This research was performed at Jet Propulsion Laboratory, California Institute of Technology under a contract with NASA, and was supported by NASA New Millennium Deep Space 1 mission and NASA Solar Electric Propulsion Technology Application

Readiness Project. Access to the Cray SV1-1A supercomputer used in this study was provided by funding from NASA Offices of Space Science, Mission to Planet Earth, and Aeronautics.

References

Brinza, D., J. Wang, J. Polk, and M. Henry, Deep Space One Measurements of Ion Propulsion Contamination, submitted to *J. Spacecraft and Rockets*, 2000.

Carruth, M., Ed., Experimental and analytical evaluation of ion thruster/spacecraft interactions, *JPL Publication* 80-92, 1981.

Carruth, M.R., A review of studies on ion thruster beam and charge-exchange plasmas *AIAA 82-1994*, 1982.

Doss, S., Miller, K., Dynamic ADI methods for elliptic equations, *Siam J. Numer. Anal.*, 16(5), 1979, pp837-855.

Douglas, J., Gunn, J., A general formulation of alternating direction methods: Part I. Parabolic and hyperbolic problems, *Numerische Mathematik*, 6, 1964, pp428-453

Gosling, J., The solar wind, *Encyclopedia of the Solar System*, Academic Press, 1999.

Hewett, D., W., Larson, D., J., Doss, S., Solution of simultaneous partial differential equations using dynamic ADI: solution of the streamlined Darwin field equations, *J. Computational Physics*, 101, 1992, pp.11-24

Katz, I., V. Davis, J. Wang, and D. Brinza, Electrical potentials in the NSTAR charge-exchange plume, *IEPC Pap.* 97-042, 1997.

Polk, J., et al., Validation of the NSTAR ion propulsion system on the Deep Space One mission: overview and initial results, *AIAA Pap.* 99-2274, 1999.

Rapp, D. and W. Francis, Charge-exchange between gaseous ions and atoms, *J. Chemical Phys.*, 37(11), 1962, pp2631.

Samanta Roy, R., D. Hastings, and N. Gatsonis, Ion-thruster modeling for backflow contamination, *J. Spacecraft and Rockets*, 33(4), 1996a, pp525.

Tajmar, M. and J. Wang, Three-dimensional numerical simulation of field-emission-electric-propulsion neutralization, *J. Propulsion and Power*, 16(3), 2000, pp536-544.

Wang, et al. Deep Space One Investigations of Ion Propulsion Plasma Environment, accepted for publication in *J. Spacecraft and Rockets*, 2000.

Wang, J., J. Brophy, and D. Brinza, 3-D simulations of NSTAR ion thruster plasma environment, *AIAA Pap.* 96-3202, 1996.

Wang, J., D. Kondrashov, P. Liewer, and S.R. Karmesin, Three-dimensional deformable-grid electromagnetic particle-in-cell for parallel computers, *J. Plasma Physics*, 61(3), 1999, pp367-389.

Wang, J., D. Kondrashov, P. Liewer, and S.R. Karmesin, Three-dimensional deformable-grid electromagnetic particle-in-cell for parallel computers, *J. Plasma Physics*, 61(3), 1999, pp367–389.

Wang, J. and D. Hastings, Ionospheric plasma flow over large high-voltage space platforms. I: Ion-plasma-time scale interactions of a plate at zero angle of attack *Physics of Fluids B*, 4(6), 1992a, pp1597–1614.

Wang, J. and D. Hastings, Ionospheric plasma flow over large high-voltage space platforms. II: The formation and structure of plasma wake, *Physics of Fluids B*, 4(6), 1992b, pp1615–1629.

VanGilder, D., G. Font, and I. Boyd, Hybrid Monte Carlo particle-in-cell simulation of an ion thruster plume, *J. Propulsion and Power* 15(4), 1999.

Table 1: Thruster operating condition from in-flight engine data

| Thrust Level | J_{b0} (A/m ²) | V_{b0} (km/s) | n_{b0} (1/cm ³) | \dot{N}_{n0} (1/s) | n_{n0} (1/cm ³) | dn_{cex0}/dt (1/cm ³ s) |
|--------------|------------------------------|-----------------|-------------------------------|----------------------|-------------------------------|--------------------------------------|
| ML 83 | 19.8 | 38.7 | 3.22×10^9 | 1.1×10^{18} | 0.23×10^{12} | 1.0×10^{13} |

Table 2: The charge-exchange plasma environment for ML83 at IDS: in-flight measurement and simulation result

| | $\Phi_p - \Phi_{scg}$ (V) | T_e (eV) | J_{cex} (A/cm ²) | n_{cex} (cm ⁻³) |
|------------|---------------------------|------------|--------------------------------|-------------------------------|
| IDS data | 19 | 2.09 | 0.9×10^{-7} | 1.2×10^6 |
| Simulation | input | input | 1.49×10^{-7} | 1.43×10^6 |

Figure Captions

Figure 1: Illustration of the Deep Space 1 spacecraft.

Figure 2: Simulation model.

Figure 3: Beam ion density, neutral plume density, and charge-exchange ion production rate on a zy plane cutting through the thruster center at $-x = 1$. a) Beam ion density (contour level: n_b/n_{b0} from 0.05 to 1 with an interval of 0.05). b) Neutral plume density (contour level: $n_n/n_{n0} = 0.025, 0.05, 0.1, 0.2, 0.4, \text{ and } 0.8$). c) Charge-exchange ion production rate ($(dn_{cex}/dt)/(dn_{cex0}/dt) = 0.005, 0.01, 0.05, 1., 0.5, \text{ and } 1.$).

Figure 4: Simulation results on a zy plane at $-x = 1$ a) Electric potential (contour clockwise from left: $\Phi - \Phi_{sc}$ from 0 to 19 v with an interval of 1 v). b) Vector plots for electric field $\vec{E}/|E|$. c) Total ion density (contour levels clockwise from left: $n_i = 10^4, 5 \times 10^4, 10^5, 5 \times 10^5, 10^6, 5 \times 10^6, 10^7, 5 \times 10^7, 10^8, 5 \times 10^8, \text{ and } 10^9$ in unit of cm^{-3}) d) Vector plots for charge-exchange ion velocity $\vec{J}_{cex}/|J_{cex}|$.

Figure 5: Simulation results on a zy plane at $-x = 10$ a) Electric potential (contour levels same as that in Figure 4) b) Vector plots for electric field $\vec{E}/|E|$. c) Total ion density (contour levels clockwise from left: $n_i = 10^4, 5 \times 10^4, 10^5, 5 \times 10^5, 10^6, \text{ and } 2 \times 10^6$ in unit of cm^{-3}). d) Vector plots for charge-exchange ion velocity $\vec{J}_{cex}/|J_{cex}|$.

Figure 6: Simulation results on a zx plane at $y = 1$ a) Electric potential (contour levels same as that in Figure 4) b) Vector plots for electric field $\vec{E}/|E|$. c) Total ion density (contour levels same as that in Figure 4) d) Vector plots for charge-exchange ion velocity $\vec{J}_{cex}/|J_{cex}|$.

Figure 7: Simulation results on a zx plane at $y = 30$ a) Electric potential (contour levels same as that in Figure 4) b) Vector plots for electric field $\vec{E}/|E|$. c) Total ion density (contour levels clockwise from left: $n_i = 5 \times 10^4, 1.5 \times 10^5, 2.5 \times 10^5, \text{ and } 3.5 \times 10^5$ in unit of cm^{-3}). d) Vector plots for charge-exchange ion velocity $\vec{J}_{cex}/|J_{cex}|$.

Figure 8: Physical quantities along several radial direction on the zx plane at $y = 1$: $z = 50$ (solid line); $z = 63$ (dashed line); $z = 37$ (dotted line); and $z = 24$ (dot-dashed line). a) Potential in Volt (The spacecraft potential is at 0 v). b) Total ion density in $1/cm^{-3}$. c) Charge-exchange ion current density in A/cm^{-2} . All length variables are normalized by the cell size of 6cm.

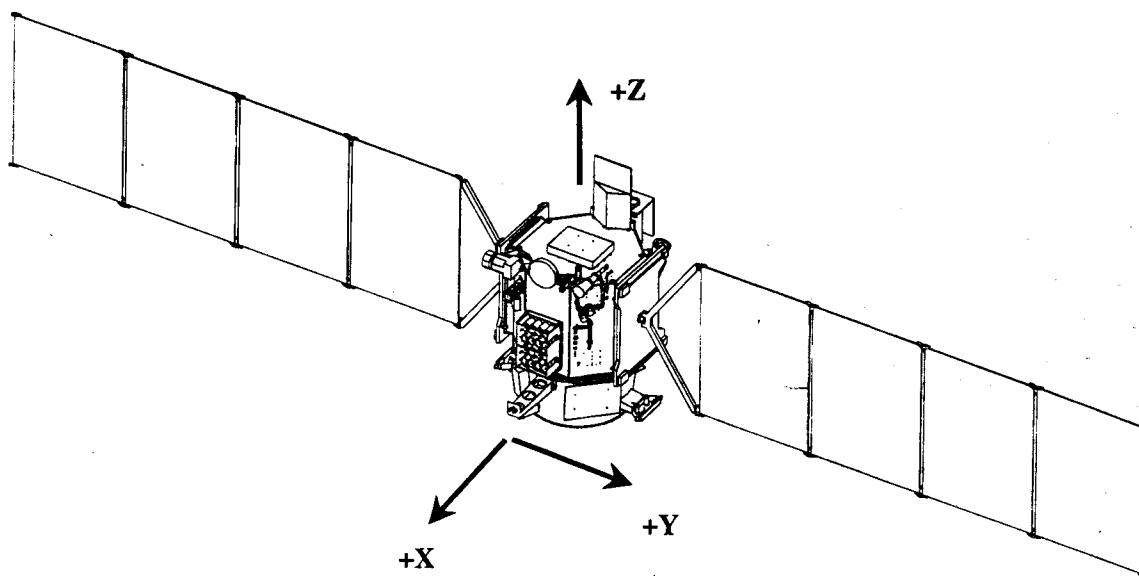


Figure 1

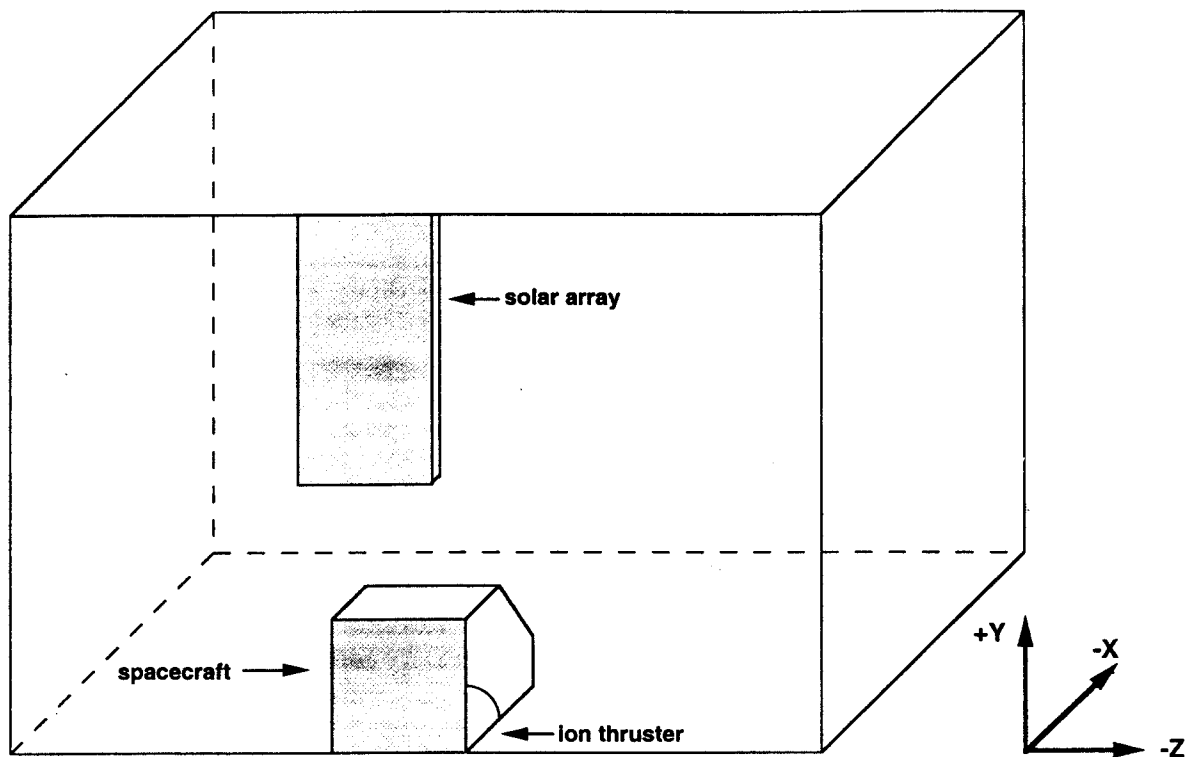


Figure 2

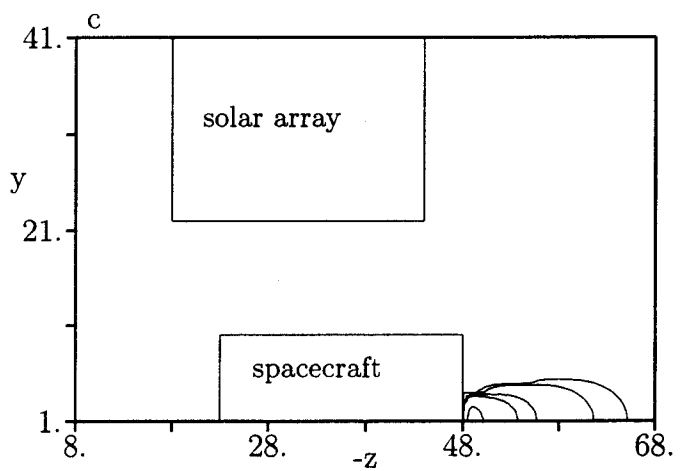
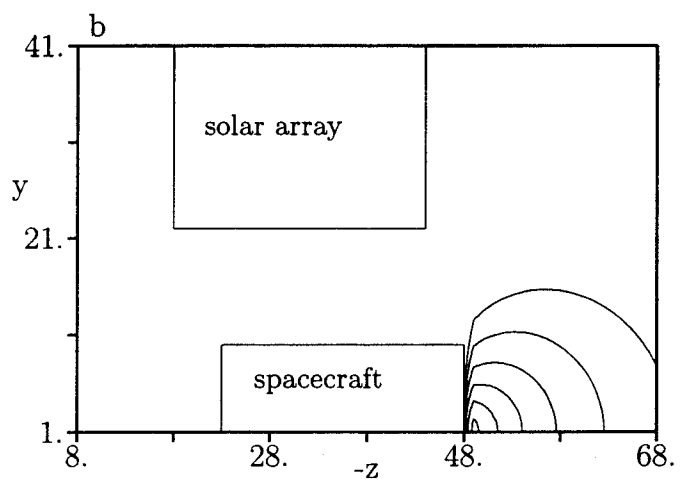
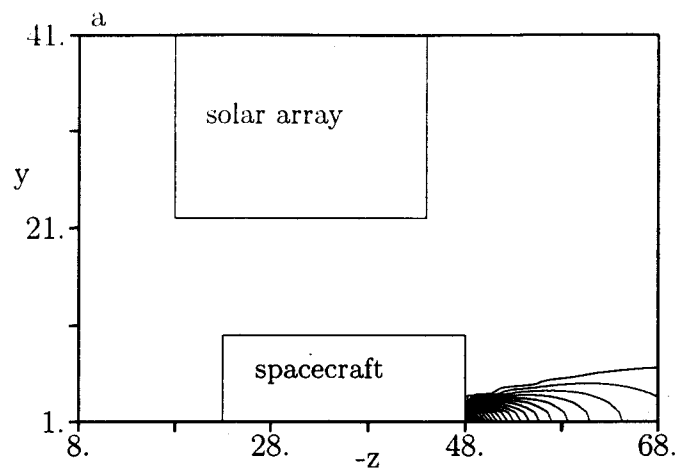


Figure 3

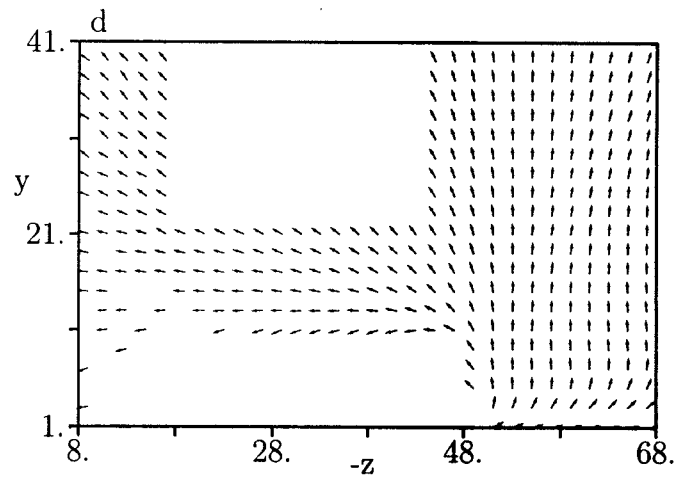
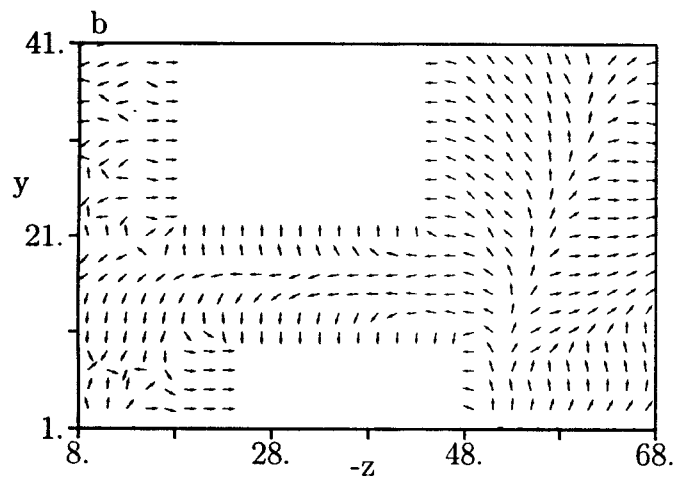
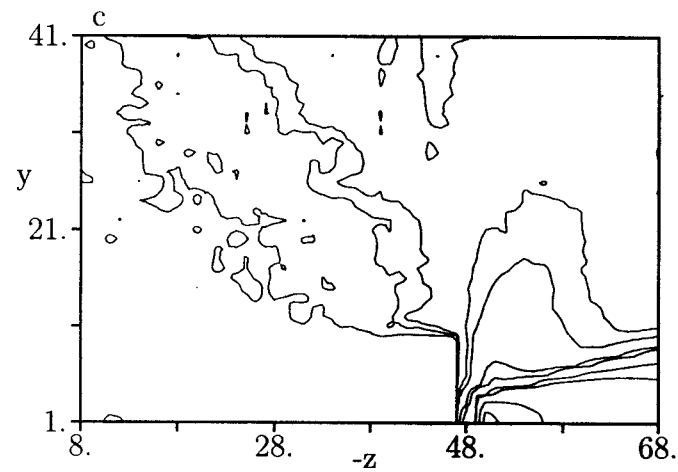
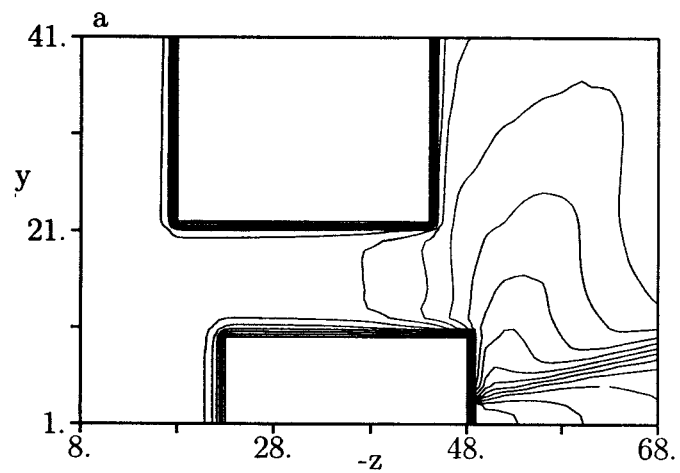


Figure 4.

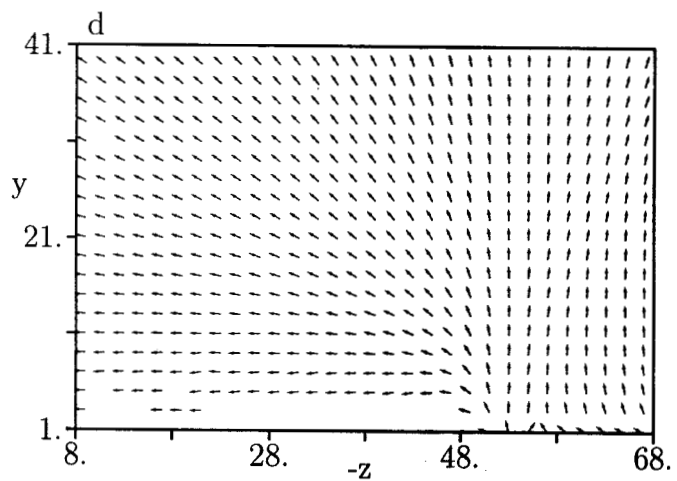
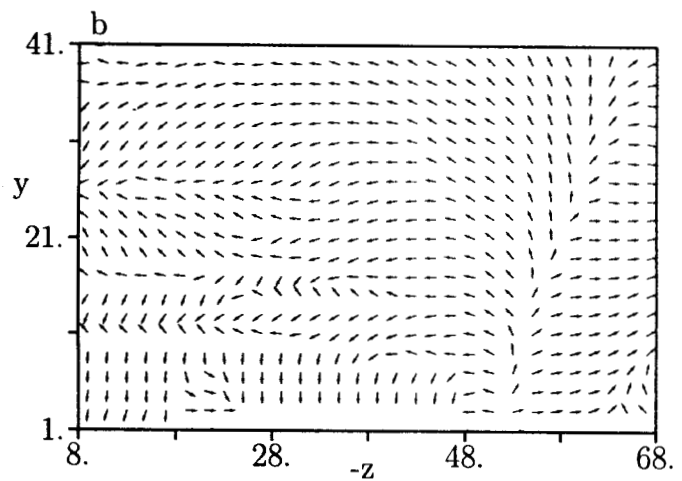
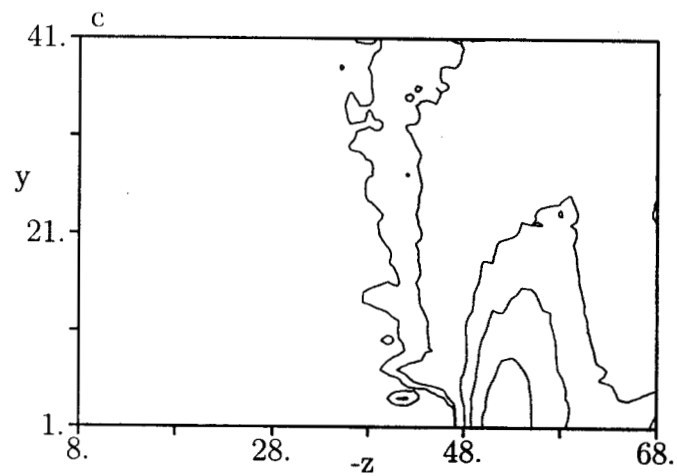
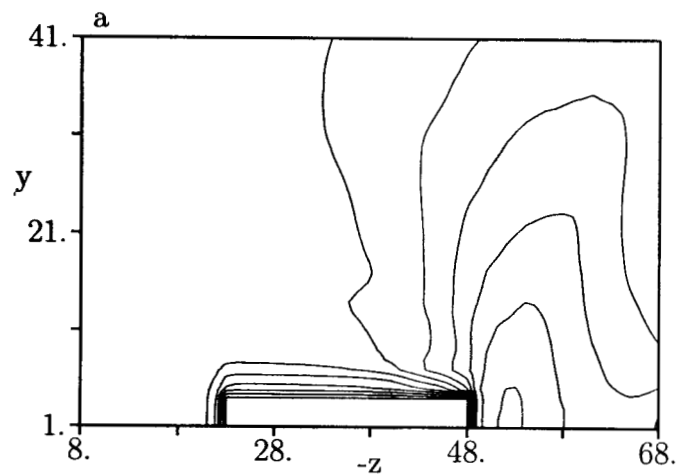


Figure 5

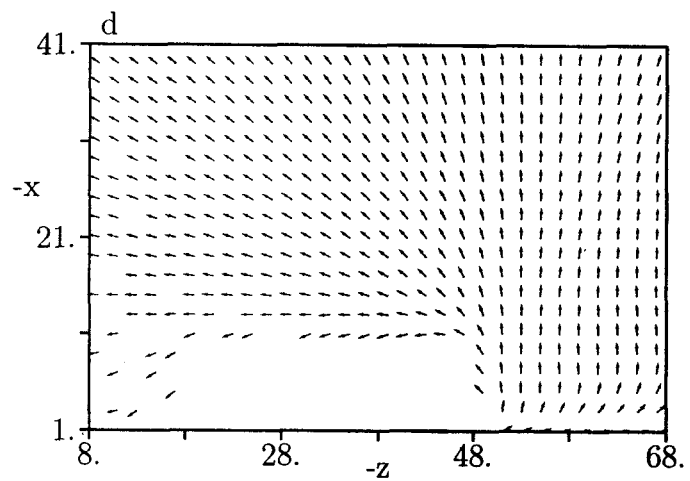
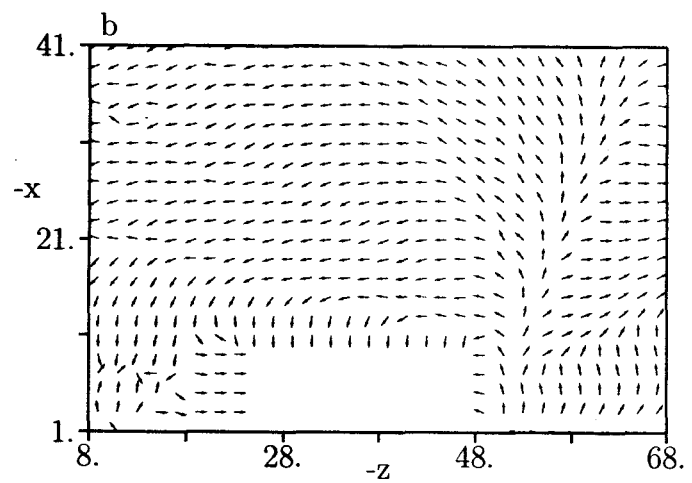
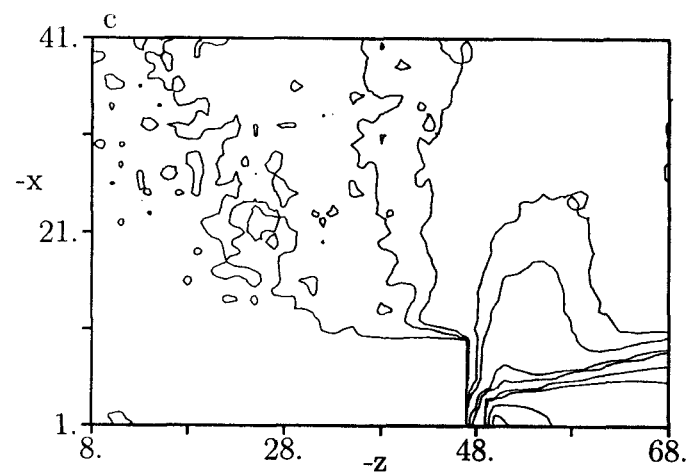
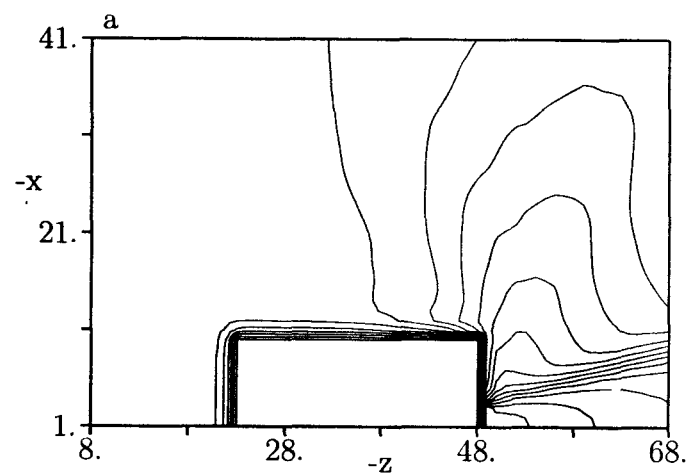


Figure 6

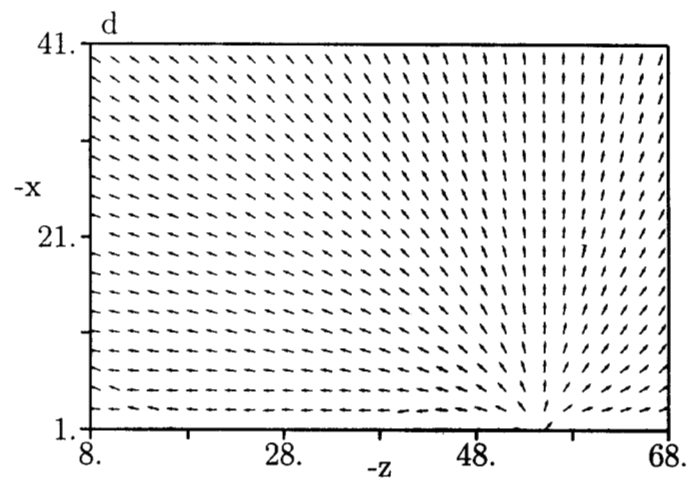
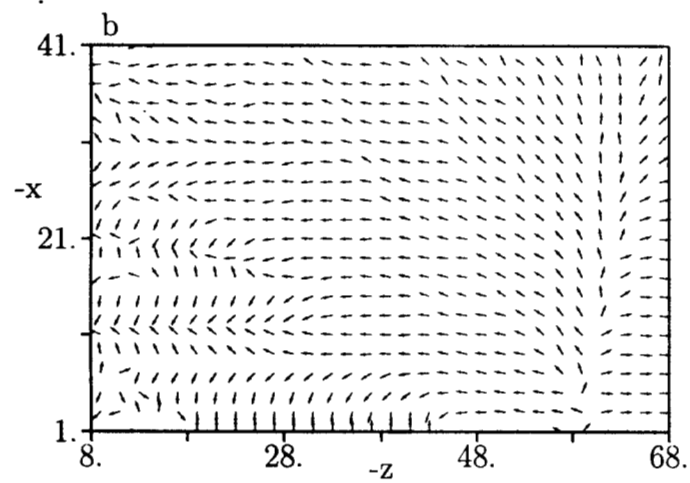
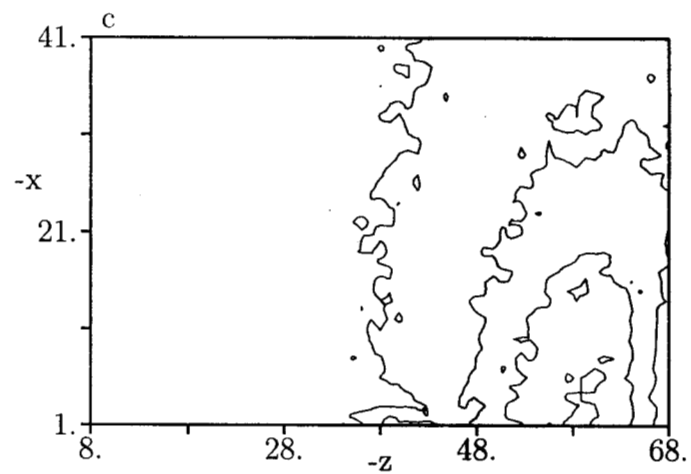
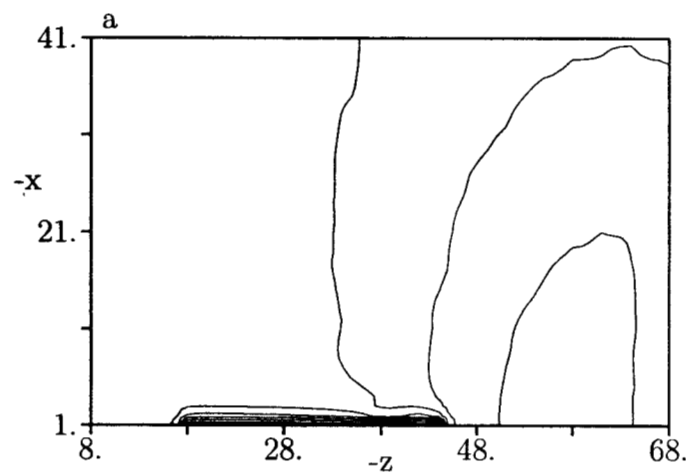


Figure 7

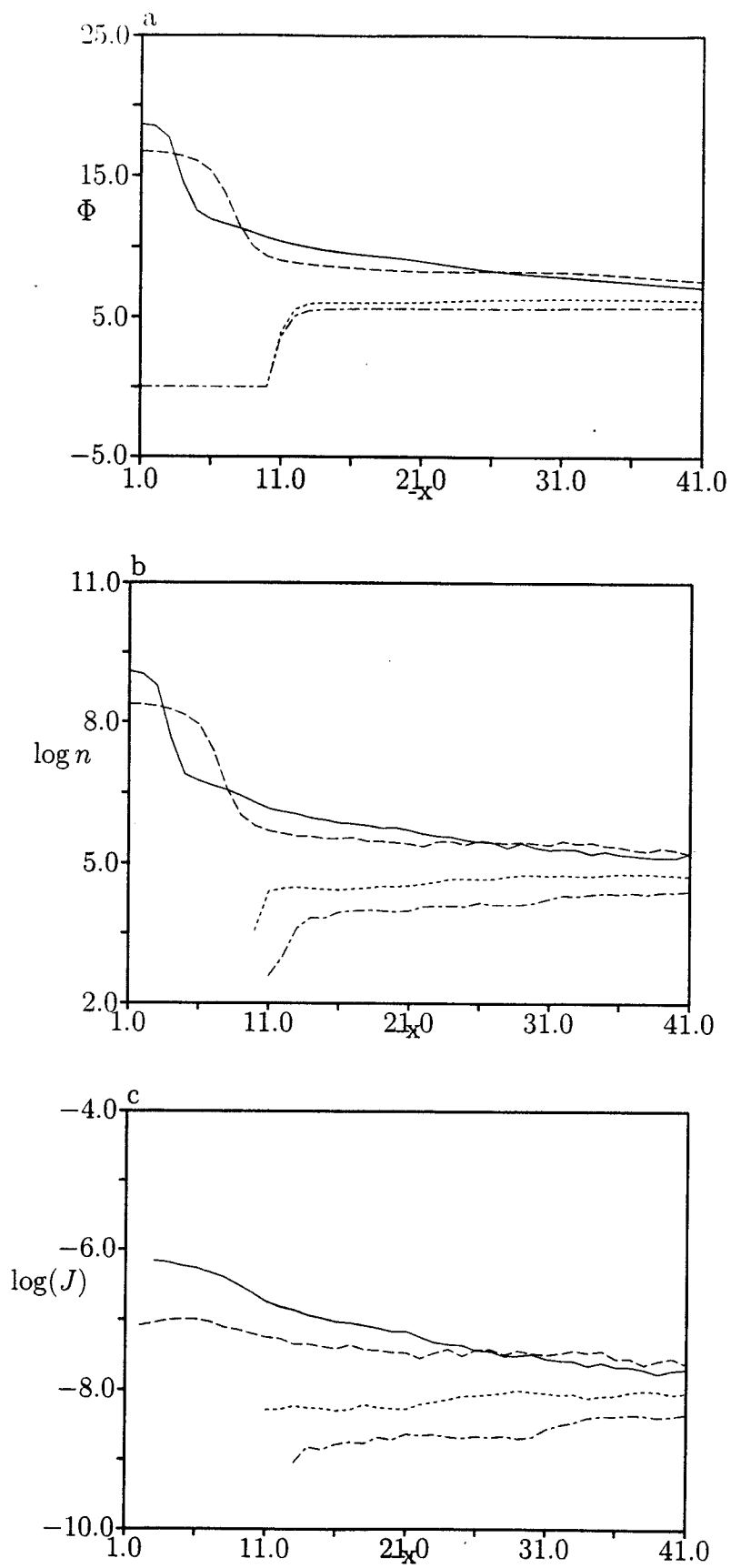


Figure 8